Carbohydrate Research, 246 (1993) 23–41
Elsevier Science Publishers B.V., Amsterdam

Conformational analysis of nitrilium intermediates in glycosylation reactions

I. Braccini, C. Derouet, J. Esnault, C. Hervé du Penhoat *, J.-M. Mallet, V. Michon and P. Sinaÿ *

Laboratoire de Chimie de l'Ecole Normale Supérieure, URA 1110, 24 rue Lhomond, 75231 Paris (France)

(Received August 18th, 1992; accepted in final form, February 24th, 1993)

ABSTRACT

In order to shed light on the stereoselectivity of acetonitrile-mediated glycosylation reactions, the nitrilium intermediates have been generated at −30°C in acetonitrile-d_3 and studied by ^1H, ^{13}C, and ^{15}N NMR spectroscopy. Conjointly, molecular modeling of the intermediates by molecular mechanics has been performed with the CHARMm force field. All the evidence suggests that only nitrilium derivatives with the α configuration are formed.

INTRODUCTION

The selective chemical synthesis of complex oligosaccharides is probably the greatest challenge in carbohydrate chemistry[1–4]. When the glycosylation reaction is performed in acetonitrile, with a non-participating protecting group at C-2 (*O*-benzyl is a typical case), β-D (or β-L) selectivity is consistently observed[1–13]. This stereochemical outcome is best explained[3,4] by formation of an α-glycopyranosylacetonitrilium ion, which then undergoes inversion of configuration upon reaction with an alcohol (Scheme 1).

In 1976, Pougny and Sinaÿ[14] were able to quench this nitrilium intermediate with *o*-chlorobenzoic acid and to isolate in high yield a stable imide, the α-configuration of which was proved by Ratcliffe and Fraser-Reid[15]. This was the first chemical evidence for the kinetic formation of a covalent anomeric nitrilium species with α-configuration. Such a transformation has subsequently been clearly demonstrated by other groups[16–19].

Lemieux has reported[20,21] that *N*-(tetra-*O*-acetyl-α-D-glucopyranosyl-4-methylpyridinium bromide exists in solution in the $B_{2,5}$ conformation, where the anomeric carbon–N^+ bond adopts an equatorial orientation. A $^1C_4$ conformation was

* Corresponding authors.

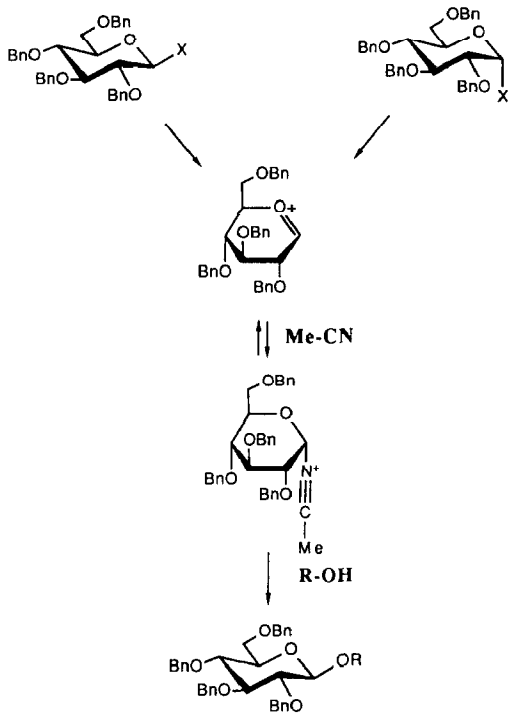

Scheme 1. Mechanism proposed for the Lewis acid catalyzed, acetonitrile-mediated glycosylation reaction.

originally claimed[22]. The object of the present work is a study of the 3D structure of the intermediate nitrilium by NMR spectroscopy and molecular modeling.

RESULTS AND DISCUSSION

Various substrates and catalysts routinely used in glycosylation reactions in this laboratory were screened for the present work. In the case of *O*-(glycosyl) trichloroacetimidates, the known rearrangement[23] to the corresponding amides was observed. The most satisfactory reaction mixtures were obtained for tetra-*O*-benzylglycosyl isopropenyl carbonates[4] in the presence of trimethylsilyl trifluoromethanesulfonate) (Scheme 2). In these cases, the solutions were homogeneous, compatible with reasonable tuning of the NMR probe.

A schematic drawing of the tetra-*O*-benzylglycopyranosides under study, along with the atomic labeling and the torsion angles of interest, is given in Fig. 1. The sign of the torsion angles is defined in agreement with the rules recommended by the IUPAC–IUB Commission of Biochemical Nomenclature[24].

Chemical shift and scalar coupling data.—NMR chemical shift and coupling constant data recorded at −30°C in acetonitrile for starting compounds with both the *gluco* (**1**; 90% α, 10% β) and *galacto* (**2**; 60% α, 40% β) configurations are

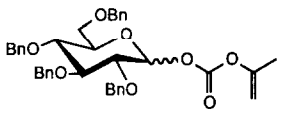

1

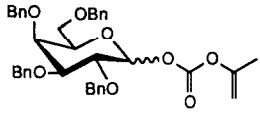

2

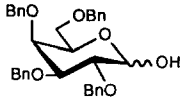

3

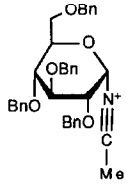

4 A,B,C

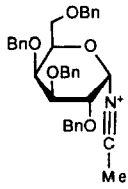

5 A,B,C

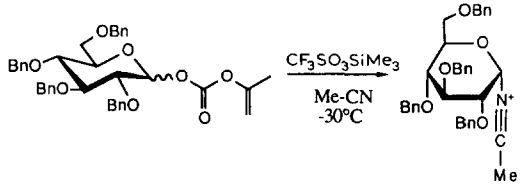

Scheme 2. Glycosyl donors, related aldoses, and reaction scheme.

collected in Tables I and II, respectively. Although the deuterated acetonitrile had been dried over molecular sieves, partial hydrolysis of intermediates to yield the corresponding tetra-*O*-benzylglycoses due to residual water could not be ruled out. Accordingly, for comparative purposes, data were also acquired for tetra-*O*-benzyl-galactoses **3**. ^{1}H NMR and ^{13}C NMR assignments for all compounds were based on homonuclear and heteronuclear correlation spectra unless stated otherwise. Vicinal proton coupling constants, $^{3}J_{H,H}$, were calculated with the equation of Altona and co-workers[25], which takes into account both the orientation and the electronegativity of the substituents. Both the experimental values and those calculated for the classical $^{4}C_{1}$ conformation are collected in Table II. The small discrepancies observed between the experimental and the calculated values suggest that the pyranose rings of these glycosyl donors adopt the $^{4}C_{1}$ conformation.

The orientation of the side chain at C-5 is described by the torsion angle ω(O-5–C-5–C-6–O-6). The distribution of rotamer populations can be determined

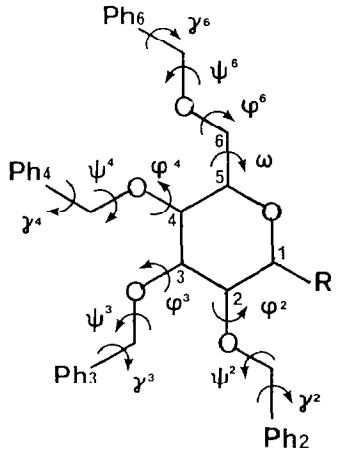

Fig. 1. Schematic drawing of tetrabenzylglycopyranosides.

TABLE I

^{1}H NMR and ^{13}C NMR chemical shift data (ppm) for compounds **1–3** in acetonitrile-d_3 at −30°C

Atom	**1α** [a]	**2α**	**2β**	**3α**	**3β**
^{1}H NMR					
Pyranose					
H-1	6.97	6.25	5.52	5.34	4.60
H-2	3.72–3.77	4.07	3.82	3.85	3.52–3.57
H-3	3.85	3.91	3.76	3.95	3.52–3.57
H-4	3.70	4.14	4.04	3.98	3.91
H-5	3.90	4.10	3.84	4.14	3.59
H-6a,6b	3.72–3.77	3.53–3.62		3.52–3.57	
Benzyl					
$-CH_2-$	4.49–4.93	4.45–4.91		4.43–4.91	
−CH=	7.20–7.43	7.30–7.50			
^{13}C NMR					
Pyranose					
C-1	93.77	94.65	97.26	90.33	96.54
C-2	78.08	74.00	77.21	75.54	79.81
C-3	80.51	77.14	73.50	77.27	81.04
C-4	75.94	73.31	72.48	74.25	73.06
C-5	72.34	71.35	74.00	68.07	72.15
C-6	67.32	67.99	67.99	68.38, 68.61	
Benzyl					
$-CH_2-$	72.15, 72.34, 74.35, 74.44	71.07, 71.35, 72.16, 72.48, 74.13, 74.30 74.59, 80.66		71.04, 71.28, 71.58 72.15, 72.15, 74.09 74.09, 74.09	
Ethylenic	102.03	101.97, 102.27			
Aromatic	127.27–138.28	127.22–138.23		127.05–138.62	

[a] Weak signals for the β isomer were also present: H-1 and H-2 at 5.62 and 3.64 ppm, respectively; carbons at 74.35, 76.40, 80.18, 83.19, 97.09, and 102.31 ppm.

TABLE II

Experimental and calculated [a] ^{1}H NMR coupling constants (Hz) for compounds **1–3**

$^3J_{H,H}$	**1α**		**2α**		**2β**		**3α**		**3β**	
	Exptl	$^4C_1$	Exptl	$^4C_1$	Exptl	$^4C_1$	Exptl	$^4C_1$	Exptl	$^4C_1$
1,2	3.4	3.0	3.7	3.0	7.8	8.2	3.6	2.8	6.8	8.1
2,3	9.5	10.0	10.2	10.0	9.8	10.0	9.9	10.0		10.0
3,4	9.5	9.7	2.7	2.8	2.7	2.8	2.8	2.8		2.8
4,5		9.9		0.8		0.8		0.8		0.8

[a] According to ref. 25.

from the values of the corresponding conformationally dependent coupling constants, $^3J_{5,6a}$ and $^3J_{5,6b}$. These coupling constants, which have been calculated for rotamers GG, GT and TG (respective values of −60, 60, and 180° for ω), are given in Table III along with the experimental values. In this terminology, the torsion angle ω(O-5–C-5–C-6–O-6) is stated first and Θ(C-4–C-5–C-6–O-6) second[26]. In the case of the *galacto* derivatives **2** and **3**, the values of the observed coupling constants suggest that the TG and GT rotamers predominate. Similar coupling constants have been reported for the hydroxymethyl moiety of α-galactose[27], the → 3)-α-D-Gal*p*(1 → residue of a human blood-group B trisaccharide[28], and methyl tetra-*O*-benzoyl-α-D-galactopyranoside[29].

When *gluco* compound **1** and $CF_3SO_3SiMe_3$ were sealed in a tube at −180°C, initial monitoring of the mixture at −30°C (10 min after thawing) indicated the presence of two major products, unchanged **1** (55%) and a new compound **4A** (45%). Within 24 h, the signals of **1** had completely disappeared and peaks corresponding to two products **4A** and **4B** were visible in the ^{1}H and ^{13}C NMR spectra (Fig. 2A). Although with time, numerous weak resonances, which could not be identified, appeared in the spectrum, the total yield (40%) of **4A** and **4B** was fairly stable. In a subsequent experiment conducted at 5°C, only the signals of a new product **4C** were observed. This transformation proved to be reversible as, upon recooling to −30°C, the signals for **4A** and **4B** were again detected. ^{1}H Chemical shift and coupling constant data for these compounds are given in Tables IV and V, respectively. With the exception of a notable difference in the chemical shift of H-1 of **4B**, 6.64 ppm, as compared to those of **4A** and **4C**, 6.21 and 6.24 ppm, respectively, all three compounds gave analogous data. The vicinal coupling

TABLE III

Experimental and calculated [a] ^{1}H NMR coupling constants (Hz) for H-6a,6b of compounds **1–3**

	Calculated [a]			Experimental				
	GG [b]	TG [b]	GT [b]	**1**	**2α**	**2β**	**3α**	**3β**
$^3J_{5,6a}$	1.1	4.9	10.8	[c]	7.3	5.9	6.4	[c]
$^3J_{5,6b}$	2.9	10.8	3.1	[c]	6.8	5.9	6.4	[c]

[a] According to ref. 25. [b] Nomenclature according to Marchessault and Perez[26]. [c] Not measured.

TABLE IV

^{1}H NMR and ^{13}C NMR chemical shift data (ppm) for compounds **4–5** in acetonitrile-d_3 at −30°C

Atom	4A	4B	4C [b]	5A	5B	5C [c]
^{1}H NMR						
Pyranose						
H-1	6.21	6.64	6.25	6.01	6.00	6.05
H-2	5.36	5.50	5.34	5.30	5.30	5.33
H-3	4.22	4.27	4.28	4.10	4.10	4.13
H-4	3.79	3.81	3.76	4.31	4.31	4.32
H-5	3.55	3.65	3.52	4.25	4.25	4.28
H-6a,6b	3.60, 3.58 [a]		3.61, 3.69	3.59, 3.66		
Benzyl						
$-CH_2-$	4.32–4.85		4.42–4.90	4.46–4.93		4.52–4.94
aromatic	7.2 –7.5		7.2 –7.6	7.2–7.5		7.2–7.5
^{13}C NMR						
Pyranose						
C-1	82.98	85.96	88.30	82.82, 82.97		83.31
C-2	80.78	78.79	79.75	88.40, 88.46		88.79
C-3	71.92	71.52	72.75	77.15		77.47
C-4	72.01		73.42	71.45		
C-5		71.68	71.28	74.98		
C-6	68.08, 68.24		69.25	67.28		67.56
Benzyl						
$-CH_2-$	78.85–70.46		72.58–71.70	74.48–70.85		75.27–71.09 [c]
aromatic	127.31–138.24		127.23–137.85	127.38–138.26		127.41–137.97

[a] From heteronuclear correlation spectrum. [b] 5°C. [c] 0°C.

constants were almost identical, indicating that the conformation of the pyranose ring was very similar for all three products. Likewise, large variations (5.32 ppm) in the chemical shifts of the signals of the anomeric carbons of **4A–C** were observed, whereas smaller differences (1–1.5 ppm) were detected for the resonances of the other ring carbons.

In the case of the *galacto* derivative **2**, 10 min after thawing (−30°C), the NMR spectrum of the mixture gave the signals of unchanged **2α** and a new compound

TABLE V

Experimental and calculated [a] ^{1}H NMR vicinal coupling constants (Hz) for compounds **4**

$^3J_{H,H}$	4A	4B	4C	4α					4β				
	Exptl	Exptl	Exptl	$^4C_1$	$_1C^4$	$^{1,4}B$	$B_{2,5}$	$^{O,3}B$	$^4C_1$	$_1C^4$	$^{1,4}B$	$B_{2,5}$	$^{O,3}B$
1,2	7.5	7.4	7.8	3.6	3.4	0.9	0.9	7.1	8.2	2.4	2.5	2.5	3.5
2,3	2.8	2.8	3.4	10.0	3.8	1.5	3.8	2.9	10.0	3.8	1.5	3.8	2.9
3,4	2.7	2.8	2.9	9.7	3.2	9.8	1.6	2.6	9.7	3.2	9.8	1.6	2.6
4,5	7.3	7.3	8.7	9.9	2.4	9.8	9.9	3.2	9.9	2.4	9.8	9.9	3.2
5,6a	6.7	6.7	5.4										
5,6b	2.9	2.9	2.4										

[a] According to ref. 25.

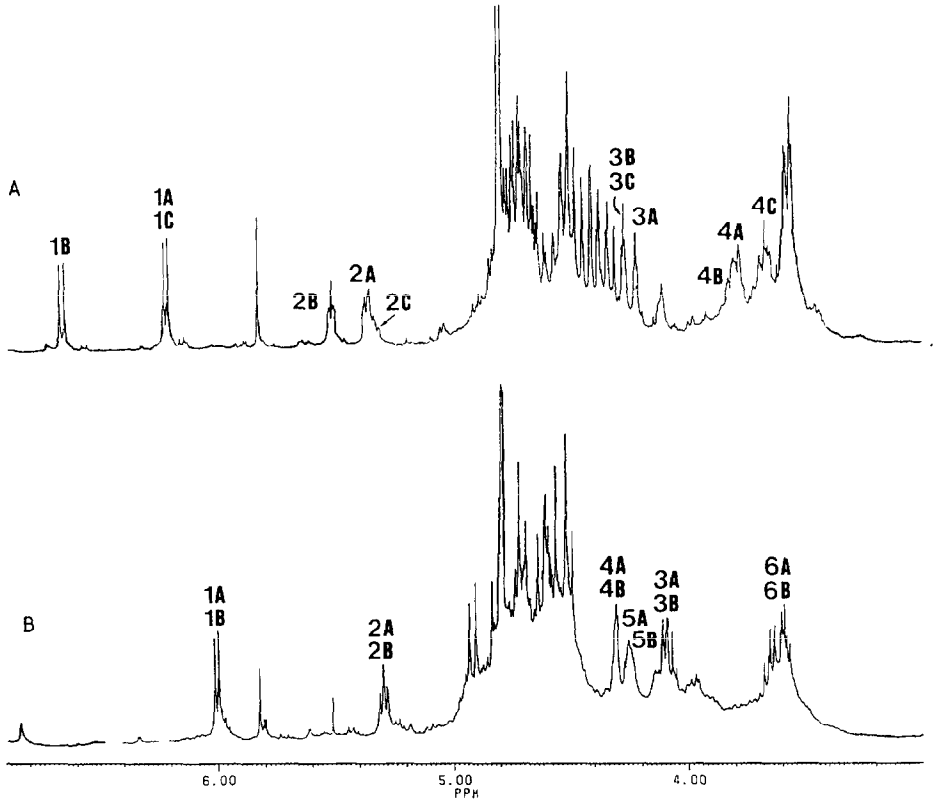

Fig. 2. ^{1}H NMR spectrum of (A) **4** and (B) **5** in acetonitrile-d_3 at −30°C.

5A. Similarly, transformation was complete within 24 h and the signals of compounds **5A** and **5B** (Fig. 2B) were detected in the NMR spectra of the mixture. An analogous reversible evolution in the NMR spectra was observed with respect to temperature as the signals of a new product, **5C**, were observed at 0°C. However, here even the chemical shifts of the H-1 and C-1 signals of the three products **5A–C** were very similar (Table IV) and again the ^{1}H coupling constants are almost identical for the three products (Table VI). Only small variations (0.3–0.5 ppm) in the chemical shifts of the ring carbons were observed for **5A–C**. Surprisingly, the chemical shifts of the C-2 signals of **5** were shifted 9 ppm to low field as compared to those of **4**. Generally speaking, the corresponding difference in chemical shifts of the C-2 carbons of galactose and glucose derivatives are small, 3 and 2 ppm for the α and β isomers, respectively[27].

The group electronegativity of the nitrilium substituent, 2.83, was calculated according to Bratch[30]. Although both a delocalized nitrilium species resulting from extensive solvent participation and an isolated acetonitrilium ion could be represented, the corresponding variations in the group electronegativity values were minor. The corresponding value for the benzyl oxygen was 3.42. $^3J_{H,H}$ Parameters

TABLE VI

Experimental and calculated [a] ^{1}H NMR coupling constants (Hz) for compounds **5**

$^3J_{H,H}$	**5A**	**5B**	**5C**	**5α**					**5β**				
	Exptl	Exptl	Exptl	$^4C_1$	$_1C^4$	$^{1,4}B$	$B_{2,5}$	$^{O,3}B$	$^4C_1$	$_1C^4$	$^{1,4}B$	$B_{2,5}$	$^{O,3}B$
1,2	6.8	6.8	6.8	3.6	3.4	0.9	0.9	7.1	8.2	2.4	2.5	2.5	3.5
2,3	6.8	6.8	7.3	10.0	3.8	1.5	3.8	2.9	10.0	3.8	1.5	3.8	2.9
3,4	1.9	1.9	2.4	2.8	2.2	3.3	8.1	3.3	2.8	2.2	3.3	8.1	3.3
4,5	3.4	3.4	2.9	0.8	3.7	0.8	0.5	8.1	0.8	3.7	0.8	0.5	8.1
5,6a	7.3	7.3											
5,6b	5.4	5.4											

[a] According to ref 25.

were established[25] for the intermediates **4** and **5** in the $^4C_1$, $^1C_4$, $B_{2,5}$, $^{O,3}B$, and $^{1,4}B$ conformations (see Fig. 3 for the boat forms[31]) and are also collected in Tables V and VI. In the case of both the α and β anomers of **4**, neither of the classical chair forms, $^4C_1$ and $_1C^4$, presented the calculated vicinal proton coupling pattern of the experimental spectra, large–small–small–large. As regards the boat forms, $^{O,3}B$ and $B_{2,5}$, the $^3J_{4,5}$ value is too low for the former while $^3J_{1,2}$ is too low

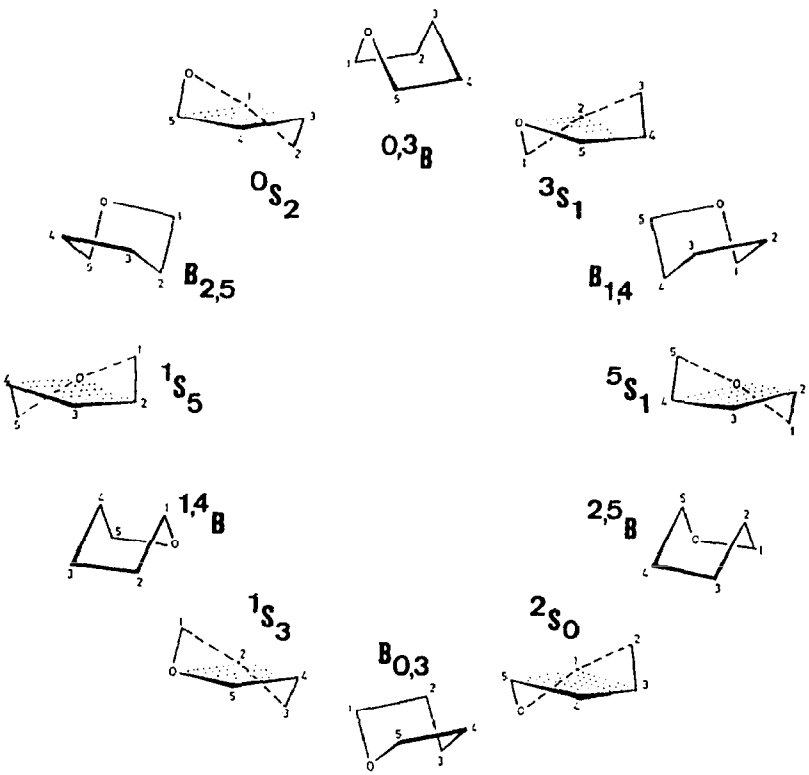

Fig. 3. Boat and skewed forms[15] for which theoretical coupling constants have been calculated.

for the latter. In the case of the *galacto* compound **5**, the best agreement between the theoretical and experimental vicinal coupling pattern (large–large–small–small) was obtained for the $\beta\ ^4C_1$ ring form. Amongst the α forms, the $^4C_1$ conformation gave the best fit, but here the $^3J_{1,2}$ value was too small. It should be noted that the vicinal coupling constants $J_{5,6a}$ and $J_{5,6b}$ of **5A** and **5B** are very similar to those of the parent compound **2**.

Equations for the calculation of four-bond coupling constants typically contain either the sum[32] of the squared cosine functions of the corresponding dihedral angles or the product[33] of the squared cosine functions of these same angles. Ranges of values of the long-range couplings of **4** and **5**, which are given in Table VII, were established from these formulae as indicated in the legend. In the case of the conformations of **4**, both the $\alpha\ ^{O,3}B$ and the $\beta\ _1C^4$ ones were expected to have a large four-bond $^4J_{2,4}$ value. However, only the former conformation gave the complete long-range coupling pattern of the experimental spectrum, medium–large–small for $^4J_{1,3}$, $^4J_{2,4}$, and $^4J_{3,5}$, respectively. As regards the *galacto* conformations, several forms have the small–small–small pattern compatible with the lack of long-range coupling in the spectrum of **5**.

It was necessary to assess the role of the solvent before proceeding with molecular modeling. If delocalization of the positive charge of the nitrogen in **4** and **5** occurred through solvent participation, this heteroatom would take on the character of an imminium species. The ^{15}N chemical shifts of **4A** and **4B** are collected in Table VIII along with the chemical shift data of related compounds[34,35]. The nitrogen chemical shifts of imines (31.7–36.4 ppm) are very different from those of either an iminium salt (158.7 ppm), acetonitrile (135.8 ppm), or nitrilium salts (238.2–252.2 ppm). Although comparisons are difficult for data obtained in such vastly different solvents, the ^{15}N shifts of **4** (195.2–233.2 ppm) lie within the range reported for nitrilium ions.

Molecular modeling.—The aim of the molecular modeling was to determine the 3D structures of the nitrilium species corresponding to local minima, close in conformational space to the structure of the oxonium precursor. In order to assess the combined molecular modeling–NMR approach with respect to tetrabenzylaldoses, **3α**, whose 3D NMR structure appeared straightforward from the vicinal coupling constants, was also studied. These calculations indicated that the ring shape for the oxonium ion was $B_{2,5}$, and a classical $^4C_1$ form was found in the case of **3α**.

Two methods, which differed only with respect to the glycosyl ring geometry, were used to explore the conformational space of the nitrilium intermediates (see Experimental). In the first approach, classical ring forms were used as starting structures and these initial geometries were subsequently allowed to evolve during minimization. With the second method, the dihedral ring angles were constrained to adopt the values calculated from the experimental proton coupling constants. The most stable structure obtained by modeling of the *gluco* intermediate **4** without constraints was the $\beta\ ^{1,4}B$ conformer (Table IX). However, the corre-

TABLE VII

Calculated [a] ^{1}H NMR long-range coupling constants (Hz) for **4** and **5**

	$^4C_1$	$_1C^4$	$^{1,4}B$	$B_{2,5}$	$^{O,3}B$	$B_{1,4}$	$^{2,5}B$	$B_{0,3}$
4								
$^4J_{1,3}\alpha$	s	s	s	s	m	s	s	s
$^4J_{1,3}\beta$	s	l	m	l	s	s	s	s
$^4J_{2,4}$	s	l	s	s	l	m	s	s
$^4J_{3,5}$	s	l	s	s	s	l	s	s
5								
$^4J_{2,4}$	s	s	m	s	s	s	s	s

[a] Key: s, small; m, medium; and l, large, calculated according to both the sum ($\cos\Theta_1^2+\cos\Theta_2^2$: $s \leqslant 1.3 \leqslant m \leqslant 1.7 \leqslant l \leqslant 2$) and the product ($\cos\Theta_1^2\times\cos\Theta_2^2$: $s \leqslant 0.3 \leqslant m \leqslant 0.7 \leqslant l \leqslant 1$) of the squared cosines of the dihedral angles Θ_1 and Θ_2.

sponding proton coupling constant data are not similar to the experimental values. In contrast, one of the stable α forms, a skewed boat $^0S_2$, presented dihedral angles almost identical to those calculated from the vicinal coupling constants. In the case of the α-starting geometries, minimization with constraints gave low-energy structures **4α-1** and **4α-2**, a flattened $^4C_1$ and a $^0S_2$ form, respectively (Table XII). On the contrary, the constrained β-starting structure evolved to a high-energy product, **4β-3**, upon minimization.

In the case of the *galacto* derivative **5**, unconstrained minimization of either α- or β-starting structures yielded $^4C_1$ forms whose coupling constants were in agreement with the experimental data (Table X). An α $^1S_3$ structure was also compatible with the data for **5**, and a β $^1S_3$ ring was the thermodynamic structure. The constrained modeling of α-starting geometries led to the minima **5α-1** and **5α-2** with forms $^1S_3$ (-22.7 kcal mol^{-1}) and $^4C_1$ (-16.0 kcal mol^{-1}), respectively; **5β-3**, a $^1S_3$ structure (-31.7 kcal mol^{-1}), was the β product obtained with constrained minimization.

TABLE VIII

^{15}N NMR chemical shifts of **4A**, **4B**, and some related compounds

Compound	Solution	Nitrogen shielding (ppm) referred to neat nitromethane	Ref
(*E*)-MeCH=CH-CH=N-*i*-Pr	Neat liquid	+31.7	34
Ph-CH=N-cyclohexyl	20% in $CDCl_3$	+36.4	34
MeC≡N	Neat liquid	+135.83	34
$CH_2=N^+Me_2\ CF_3COO^-$	In $CHCl_2CHCl_2$	+158.7	34
MeC≡N$^+$H	$FSO_3H-SbF_5-SO_2$ Solution at -60°C	+238.23	35
	10% (v/v) in 90%H_2SO_4	+252.2	34
4A+4B	MeCN+$CF_3SO_3SiMe_3$, -30°C	+195.15, 220.69, 223.16, 233.21	

TABLE IX

Experimental and calculated [a] (approximate geometry) ^{1}H NMR coupling constants (Hz) for low-energy conformations of compounds **4** minimized without constraints

	4A	**4B**	**4C**	**4α**			**4β**		
	Exptl	Exptl	Exptl	$^4C_1$	$_1C^4$	$^0S_2$	$^4C_1$	$_1C^4$	$^{1,4}B$
$^3J_{H,H}$									
1,2	7.5	7.4	7.8	7.2	1.4	7.1	8.9	2.1	3.2
2,3	2.8	2.8	3.4	3.5	2.1	0.5	8.5	3.3	2.1
3,4	2.7	2.8	2.9	6.6	2.4	2.5	6.0	2.7	1.4
4,5	7.3	7.3	8.7	9.7	1.6	9.9	8.0	0.8	6.2
5,6a	6.7	6.7	5.4	10.3	11.1	10.3	11.0	7.3	0.7
5,6b	2.9	2.9	2.4	3.0	5.9	2.8	3.7	8.4	4.0
$^4J_{H,H}$									
1,3	+	+		s	s	s	s	l	l
2,4	2.4	2.4	1.0	s	l	s	s	l	s
3,5				s	l	s	s	l	s
Energy [b]				−27.4	−20.3	−26.9	−16.6	−35.8	−43.5

[a] See the footnotes of Tables V and VII. [b] kcal/mol.

It is to be noted that several of the structures obtained by constrained minimization, **4α-1**, **4β-3**, and **5β-3**, were not local minima and evolved to very different ring forms when the constraint energy term was removed from the force field. The modelized structures obtained with constraints are shown in Fig. 4.

Relaxation data.—Approximate tumbling times (τ_c) of 0.31, 0.35, and 0.25 ns were calculated for **3–5** from the average T_1 values of the methine carbons. In the

TABLE X

Experimental and calculated [a] (approximate geometry) ^{1}H NMR coupling constants (Hz) for low-energy conformations of compounds **5** minimized without constraints

	5A	**5B**	**5C**	**5α**			**5β**		
	Exptl	Exptl	Exptl	$^4C_1$	$_1C^4$	$^1S_3$	$^4C_1$	$_1C^4$	$^1S_3$
$^3J_{H,H}$									
1,2	6.8	6.8	6.8	5.9	1.5	4.8	8.9	2.1	1.0
2,3	6.8	6.8	7.3	8.5	3.0	7.2	8.5	3.3	4.5
3,4	1.9	1.9	2.4	2.7	3.3	1.8	2.2	4.2	2.9
4,5	3.4	3.4	2.9	0.3	5.5	4.3	0.4	7.3	3.3
5,6a	7.3	7.3		9.9	11.0	9.4	10.9	7.4	0.9
5,6b	5.4	5.4		2.4	6.0	7.8	3.6	8.6	6.1
$^4J_{H,H}$									
1,3				s	s	s	s	l	s
2,4			0.5	s	s	s	s	s	s
3,5				s	m	s	s	l	s
Energy [b]				−26.7	−18.4	−26.3	−22.9	−47.7	−54.6

[a] See the footnotes of Tables V and VII. [b] kcal/mol.

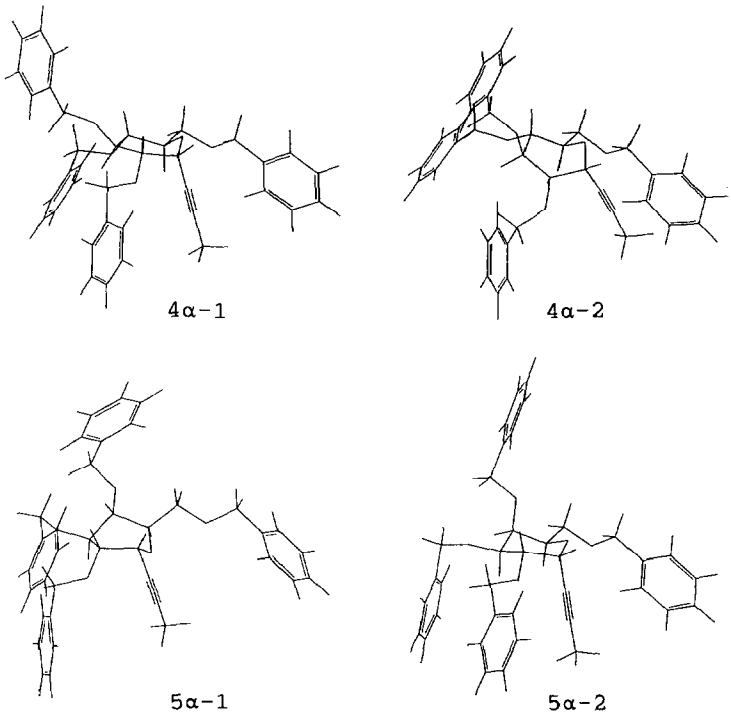

Fig. 4. Constrained minima of α-nitrilium intermediates **4** and **5**.

case of **3α**, a definitive value of 0.33 ns for τ_c was obtained from a fit of the theoretical and observed negative intraresidue cross-peaks[36]. These correlation times implied very weak dipolar coupling. However, as the relaxation rates of the anomeric protons of carbohydrates are generally very different for the two anomers, the diagonal volumes are an excellent probe of the configuration at C-1[37,38].

TABLE XI

Calculated [a] and (experimental) normalized NOESY volumes (a_{ij}) for **3α**

Spin	$a_{i,j}$				
	H-1	H-2	H-3	H-4	H-5
H-1	0.52	−0.014			
	(0.49)	(−0.02)			
H-2		0.45	−0.003		
		(0.55)	(−0.02)		
H-3			0.46	−0.008	−0.014
			(0.43)	(-0.008)	(−0.008)
H-4				0.28	−0.008
				(0.37)	(−0.006)
H-5					0.42
					(0.43)

[a] $^4C_1$, 36 kcal mol^{-1}.

TABLE XII

Ring form (energy [a]) and theoretical normalized NOESY volumes (a_{ij}) for constrained minima of **4** and the corresponding experimental volumes

τ_m (s)	$a_{i,j}$	Calculated			Experimental
		4α-1 $^4C_1$ (−20.0)	**4α-2** $^0S_2$ (−17.9)	**4β-3** $^4C_1$ (−12.4)	**4A**
0.5					
	$a_{1,1}$	0.65	0.70	0.68	0.61
	$a_{2,2}$	0.50	0.55	0.66	
	$a_{3,3}$	0.39	0.20	0.41	0.27
1.0					
	$a_{1,1}$	0.42	0.50	0.46	0.41
	$a_{2,2}$	0.25	0.31	0.43	0.20
	$a_{3,3}$	0.15	0.04	0.17	0.18

[a] kcal mol^{-1}.

Phase-sensitive NOESY spectra were recorded for mixing times of 0, 0.5, and 1 s (1 s only for **4** and **5**). Several diagonal and cross-peak volumes were extracted from the experimental spectrum of **3** (Table XI). In the case of **4** and **5**, comparison of the relative intensities of the solvent and sugar signals in spectra recorded before and after the NOESY experiments showed that, amongst the nitrilium intermediates, only the concentration of **4A** was constant throughout these experiments. Accordingly, diagonal volumes for H-1, H-2, and H-3 of **4a** were extracted from these experimental spectra and are collected in Table XII.

Combination of NMR and modeling results.—It has been shown recently, in the case of sucrose, that averaging of the internuclear distances over all of conformational space is required in order to obtain a good fit between calculated and experimental relaxation data[39]. As complete mapping was not feasible in the present work, comparisons have been made with respect to minima structures. Moreover, isotropic tumbling in the absence of internal motion has been assumed. This approximation is undoubtedly justified as regards the sugar ring[40]. However, data are lacking for a reasonable estimation of the rate of internal motion of the pendant benzyl groups at −30°C. From relaxation data obtained at several temperatures, the internal motion of the pendant methyl group of methyl 3-*O*-α-D-rhamnopyranosyl-α-D-glucopyranoside (> 0°C) has been shown to be fast (a factor of 10–50) compared to the overall motion[41]. The relative rates of internal and overall motion determine the appropriate averaging procedure[42], but the lack of stability of the nitrilium intermediates precluded the extensive measurements required in order to establish these rates.

The agreement between the theoretical and experimental diagonal volumes for H-1 of **3α** was excellent (Table XI). As a result of relaxation to external sources, diagonal volumes calculated with a leakage rate, R_{li}, set to 0 as in Tables XI and XII, are typically larger (~ 5–20%) than experimental values. A poorer fit was

obtained for the diagonal volumes of H-2 to H-4 of compound **3**, as the calculated volumes were smaller than the experimental values. Moreover, as the number of efficient relaxation interactions between the sugar protons and the benzyl methylene protons increased, the difference between the corresponding calculated and observed diagonal volumes increased. It is possible that vacuum modeling of the tetrabenzylglycosides overemphasizes the attractive forces between the benzyl groups and the sugar ring. The resulting internuclear distances would be too small, leading to reduced diagonal volumes for the modeled structures. Upon increasing the value of the dielectric constant from 1 to 4, minimization of **3α**, **4α-1**, and **5α-1** effectively led to minima structures that were more extended. The ring geometries did not vary during the latter calculations. Some flexibility was to be expected for the benzyl side-chains. Indeed, the modeling had revealed low-energy conformers with more extended benzyl groups, and thus averaging would also be expected to lead to larger apparent distances and in turn larger calculated diagonal volumes. Finally, a reasonable fit between the theoretical and observed negative cross-peak volumes of **3α** was obtained, considering the low intensities of these signals.

The calculated diagonal volumes for H-1 of all the constrained minima of **4** are in good agreement with the experimental data (5–20% larger). The relaxation of the anomeric proton with the benzyl protons was not efficient ($r_{1,Bn2} > 4.2$ Å, whereas $r_{1,2} = 2.2$ Å) for any of the low-energy structures. In order to obtain a rough estimate of the effect of internal motion of the benzyl group at O-2 on the calculated diagonal volumes of H-1 of **4α-2**, a volume matrix was calculated for a low-energy conformer with a larger H-2–Bn2 distance ($r_{2,Bn2}$ 3.7 Å instead of 2.9 Å). This calculation produced only a minor variation in the H-1 volume (1%). Although a poorer fit could be anticipated for the $\mathbf{a}_{2,2}$ and $\mathbf{a}_{3,3}$ values due to both the vacuum-modeling and the neglect of internal motion, they reproduce the experimental data reasonably well.

Both the reverse anomeric effect and the large bulk of the pyridinium group have been evoked to account for the conformational preference of *N*-(tetra-*O*-acetyl-α-D-glucopyranosyl)-4-methylpyridinium bromide[21]. The only low-energy structures with a conformation compatible with the reverse anomeric effect, which places the positively charged nitrogen atom between the O-5 lone pairs in the Newman projection along the C-1–O-5 axis, are **4β-3** and **5α-1**; the former is a structure that is unstable in the absence of the dihedral constraint energy term, while the other minimum is relatively stable. Moreover, the orientation of the acetonitrile substituent of the *α-gluco* minima structures is always axial in contrast to the equatorial orientation of the pyridinium group of *N*-(tetra-*O*-acetyl-α-D-glucopyranosyl)-4-methylpyridinium bromide. The steric requirement of the linear acetonitrile group is of course much smaller than that of the pyridinium moiety.

Clearly, for nitrilium intermediate **4**, the NMR relaxation data and vicinal coupling constants are well modeled by both α and β constrained minima. However, only the **4α-2** structure corresponds to both a local minima and reproduces the observed long-range proton coupling constants (m, m-1, and s for $^4J_{1,3}$,

$^4J_{2,4}$, and $^4J_{3,5}$, respectively). In the case of **5**, amongst the constrained structures reproducing the experimental data, only the α-geometries **5α-1** and **5α-2** are stable. The rotamer populations of the nitrilium intermediates obtained from the $J_{5,6a}$ and the $J_{5,6b}$ coupling constants are typical of the parent aldoses. Accordingly, it would appear improbable that the multiple conformers observed at −30°C are rotamers. Although it has been shown by molecular mechanics that the β isomer is much more stable than the α isomer, conversion of the kinetic product into the thermodynamic one is not observed. It is possible that variations in the orientations of the pendant groups are responsible for the existence of multiple conformers which interconvert slowly on the NMR timescale at −30°C.

EXPERIMENTAL

NMR spectroscopy.—Spectra were recorded on a Bruker AM-400 spectrometer operating in the FT mode at 400.13 MHz for ^{1}H, 100.57 MHz for ^{13}C, and 40.54 MHz for ^{15}N. Approximately 50 (200) mg of glycosyl compound[4] and 1 equiv of $CF_3SO_3SiMe_3$ (where indicated) were sealed in 5(10)-mm NMR tubes in MeCN-d_3 at −180°C. Deuterated MeCN was the internal standard (δ_H 2.0 ppm, δ_C 0.3 ppm, and δ_N 135.8 ppm). The spectral window for the ^{1}H NMR spectra was 10 ppm for 16K data points with a pulse width of 8 μs (45°), an 8-s delay between each scan, and an acquisition time of 2 s. ^{13}C NMR spectra were recorded with a spectral window of 30000 Hz, complete proton decoupling, and a pulse width of 8 μs (60°). The acquisition time was 1.11 s with a 1.5-s delay between each scan. ^{15}N NMR spectra were recorded without proton decoupling, a spectral width of 20000 Hz, and a pulse width of 10 μs (45°). The acquisition time was 0.8 s and a 5-s delay was introduced prior to each scan. Standard sequences were used for the [δ–δ, ^{1}H–^{1}H]COSY, [δ–δ, ^{1}H–^{13}C]COSY, [δ–δ, ^{1}H–^{1}H]COSYLR, phase-sensitive DQFCOSY and NOESY spectra. The delay value for the long-range experiment was 0.1 s.

In the case of phase-sensitive NOESY spectra, a 20-ms variable delay was introduced at the beginning of the mixing time in order to suppress *J*-peak transfer. The recycle time was set to 5 times the longest T_1 in order to ensure that the normalized NOESY volume matrix would be symmetrical. 512 × 1K data matrices were obtained and zero-filled to 1K × 1K. Prior to Fourier transformation, the first data file was halved to reduce T_1 ridges, and $\pi/2$-shifted squared sine-bell weighting functions were applied[43]. NOESY volumes were evaluated from the summed w_1 subspectra contributing to a specific signal and normalized with respect to the spectrum acquired with a mixing time of 0 s.

Molecular modeling.—The molecular modeling was performed with the standard CHARMm force field, and a dielectric constant of unity was used. It was not possible to use the parameters optimized for carbohydrates[44] in the calculations as, under these conditions, most of the skew and boat forms of the pyranose ring were unstable and reverted to chair forms. New atom types for both the carbon

and oxygen atoms of the oxonium ion were created, using parameters from a theoretical study[45]. The lengths of the C–O bond in the various oxycarbocation species reported in this study were calculated to be 1.23–1.28 Å, which is closer to the length of the carbonyl bond (1.20 Å) than to that of an ether linkage (1.41 Å). Accordingly, during modeling, the cyclic substituents attached to the C–O bond were constrained to adopt planar geometry. The charge distribution was evaluated with the CINDO routine of the Quanta package.

The nitrilium moiety was modeled from the MeCN fragment in the CHARMm data set with a formal positive charge of 1*e* localized on the nitrogen atom in keeping with the ^{15}N chemical shift. Attention has been drawn to the importance of electrostatic forces in pyranose conformations in a recent study of the boat–chair transition of chondrosine induced by electrostatic interactions[46]. In the absence of parameters from theoretical studies, a more satisfying model for the nitrilium species could not be elaborated although, clearly, this would be desirable. Initial geometries for the benzyl fragment and, when possible, the sugar rings were taken from the CHARMm data set.

A range of starting conformations for both anomeric forms of the pyranoid ring were imposed by altering the relevant dihedral angles. Both boat conformations close to that of the oxonium precursor ($^{1,4}B$, $B_{2,5}$, and $^{O,3}B$) and the classical chair forms ($^4C_1$ and $^1C_4$) were included. Minimization was performed with the CHARMm force field, which includes potential energy terms arising from electrostatic, stretching, bending, torsional, and hydrogen bonding contributions. The computer time required for complete mapping in 30° steps of the conformational space of the thirteen torsion angles of the benzyl groups alone was prohibitive (10^{14} conformations), and thus two semi-systematic search protocols for the torsion angles closest to the sugar ring were used.

In the first method, the starting structure was minimized with both conjugate-gradient and adopted basis Newton–Raphson methods prior to mapping the conformational space of the benzyl moieties in steps of 30° for φ^2, ψ^2, φ^3, and ψ^3 (20736 conformations from 12 searches). As ψ^2 and ψ^3 values of 180° were invariably observed for the low-energy conformers, in subsequent searches the ψ^2, ψ^3, and ψ^4 torsions were fixed at 180° while the φ^2, φ^3, and φ^4 angles were mapped in steps of 30°. Next, a systematic search about the ψ torsion angles (ψ^2, ψ^3, and ψ^4) was performed using the values of φ^2, φ^3, and φ^4 previously optimized. The primary hydroxyl group was mapped alone (ω, φ^6, and ψ^6). Finally, the orientations of the benzene groups (γ angles) were optimized with gridscan searches in steps of 10°. Several of the low-energy conformers of **3**–**5** from each search were minimized.

In the second approach, which has been applied to **4** and **5**, all starting geometries were elaborated from basic atom types. The sugar ring was then forced to adopt the form corresponding to the dihedral angles calculated from the experimental vicinal coupling constants of **4** and **5**. This was achieved by imposing dihedral constraints which were included in the form of extra energy terms. The

torsion angles of the benzyl groups were then incremented in a systematic manner as described above.

Calculations of rotational correlation times and NOESY volumes.—Approximate values of the tumbling times, τ_c, were calculated from the average T_1 of the methine carbons, according to the following equation,

$$\frac{1}{T_1} = \frac{1\hbar^2\gamma_C^2\gamma_H^2}{10r_{C-H}^6}\left\{\frac{\tau_C}{1+(\omega_H-\omega_C)^2\tau_C^2}+\frac{3\tau_C}{1+\omega_C^2\tau_C^2}+\frac{6\tau_C}{1+(\omega_H+\omega_C)^2\tau_C^2}\right\}$$

where, $\hbar$ is Planck's constant divided by 2π, γ_C and γ_H are the carbon and proton magnetogyric ratios, respectively. τ_c is the rotational correlation time, and r_{C-H} is the proton–carbon distance which was assumed to be 0.11 nm.

Theoretical NOESY volumes for mixing times of 0.5 and 1 s were calculated for low-energy structures of **3α** (only 0.5 s), **4α-1**, **4α-2**, and **4β-3** from the corresponding internuclear distances, using in-house software. This routine uses the full-matrix approach[47]. For a multi-spin system, the integrated intensity of a cross-peak between two protons i and j in a NOESY spectrum is described as follows

$$V_{\tau m} = V_0\, e^{-\Gamma\cdot\tau_m}$$

where V_0 and $V_{\tau m}$ are the matrix of peak volumes for mixing times of 0 and τ_m s, respectively, and Γ is the relaxation matrix.

$$\Gamma = \begin{bmatrix} R_{11} & R_{12} & R_{13} & . & . \\ R_{21} & R_{22} & . & . & . \\ . & . & . & . & . \\ . & . & . & . & R_{nn} \end{bmatrix}$$

This equation is solved by rewriting it in terms of the matrix of eigenvectors, $[X]$, and the diagonal matrix of eigenvalues, $[D]$, of $V_{\tau m}\cdot V_0^{-1}$.

$$\Gamma = -[X]\ln[D][X]^{-1}/\tau_m$$

The relaxation constants, R_{ii} and R_{ij}, have been calculated from the transition probabilities as follows

$$R_{ii} = \sum_j\left(W_0^{ij} + 2W_1^{ij} + W_2^{ij}\right) + R_{li}$$

$$R_{ij} = \left(W_2^{ij} - W_0^{ij}\right)$$

where W_0, W_1, and W_2 are the zero-, single-, and double-quantum transition probabilities, and R_{li} is a leak relaxation of nuclei i to external sources. The transition probabilities are in turn written as

$$W_0^{ij} = q_{ij}J(\omega_i - \omega_j)$$

$$W_1^{ij} = 1.5q_{ij}J(\omega_i)$$

$$W_2^{ij} = 6q_{ij}J(\omega_i + \omega_j)$$

where $J(\omega)$ is the spectral density function describing the motion of the dipolar coupled nuclei. The algorithm includes various spectral density functions appropriate for different models of molecular motion. In the present study, isotropic tumbling in the absence of internal motion was assumed and thus

$$q_{ij} = 0.1\gamma_H{}^4(h/2\pi)^2 r_{ij}^{-6}$$

$$J(\omega) = \tau_c/1 + \omega^2\tau_c^2$$

ACKNOWLEDGMENTS

One of us (I.B.) acknowledges support from the French Ministry of Research and Technology. We thank the Pierre and Marie Curie University (Paris VI) and the C.N.R.S. (URA 1110) for financial help.

REFERENCES

1 H. Paulsen, *Angew. Chem. Int. Ed. Engl.*, 21 (1982) 155–224.
2 R.R. Schmidt, *Angew. Chem. Int. Ed. Engl.*, 25 (1986) 212–235.
3 P. Sinaÿ, *Pure Appl. Chem.*, 63 (1991) 519–528.
4 A. Marra, J. Esnault, A. Veyrières, and P. Sinaÿ, *J. Am. Chem. Soc.*, 114 (1992) 6354–6360, and references therein.
5 A. Marra, J.-M. Mallet, C. Amatore, and P. Sinaÿ, *Synlett*, (1990) 572–574.
6 S. Hashimoto, T. Honda, and S. Ikegami, *J. Chem. Soc., Chem. Commun.*, (1989) 685–687.
7 S. Hashimoto, M. Hayashi, and R. Noyori, *Tetrahedron Lett.*, 25 (1984) 1379–1382.
8 R.R. Schmidt, M. Behrendt, and A. Toepfer, *Synlett*, (1990) 694–696.
9 R.R. Schmidt and E. Rücker, *Tetrahedron Lett.*, (1980) 1421–1424.
10 T. Murose, K. Kameyama, P.R. Kortha, H. Ishida, M. Kiso, and A. Mossegrowe, *J. Carbohydr. Chem.*, 8 (1989) 265–283.
11 A. Marra and P. Sinaÿ, *Carbohydr. Res.*, 195 (1990) 303–308.
12 A. Marra, F. Gauffeney, and P. Sinaÿ, *Tetrahedron*, 47 (1991) 5149–5160.
13 S. Hashimoto, Y. Yonagiya, T. Honda, H. Harada, and S. Ikegami, *Tetrahedron Lett.*, 33 (1992) 3523–3526.
14 J.-R. Pougny and P. Sinaÿ, *Tetrahedron Lett.*, (1976) 4073–4076.
15 A.J. Ratcliffe and B. Fraser-Reid, *J. Chem. Soc., Perkin Trans.* 1, (1990) 747–750.
16 R.U. Lemieux and R.M. Ratcliffe, *Can. J. Chem.*, 57 (1979) 1244–1251.
17 A.A. Poira, S.N. Ung-Chhun, and J.-L. Durand, *J. Org. Chem.*, 46 (1981) 3158–3160.
18 A. Klemer and M. Kohla, *J. Carbohydr. Chem.*, 7 (1988) 785–797.
19 D.M. Gordon and S.J. Danishefsky, *J. Org. Chem.*, 56 (1991) 3713–3715.
20 R.U. Lemieux, *Pure Appl. Chem.*, 27 (1971) 527–547.
21 R.U. Lemieux, K.B. Hendriks, R.V. Stick, and K. James, *J. Am. Chem. Soc.*, 77 (1975) 4056–4062.
22 R.U. Lemieux and A.R. Morgan, *Can. J. Chem.*, 43 (1965) 2205–2213.
23 H.G. Hoffmann and R.R. Schmidt, *Liebigs Ann. Chem.*, (1985) 2403–2409.
24 IUPAC–IUB Commission on Biochemical Nomenclature, *J. Mol. Biol.*, 52 (1970) 1–17.
25 C.A.G. Haasnoot, F.A.A.M. de Leeuw, and C. Altona, *Tetrahedron*, 36 (1980) 2783–2792.
26 R.H. Marchessault and S. Perez, *Biopolymers*, 18 (1979) 2369–2374.
27 K. Bock and H. Thogersen, *Annu. Rep. NMR Spectrosc.*, 13 (1982) 1.
28 H. Thogersen, R.U. Lemieux, K. Bock, and B. Meyer, *Can. J. Chem.*, 60 (1982) 44.
29 Y. Nishida, H. Ohrui, and H. Meguro, *Tetrahedron Lett.*, 25 (1984) 1575–1578.
30 S.G. Bratsch, *J. Chem. Educ.*, 62 (1985) 101–103.
31 J.C.P. Schwarz, *J. Chem. Soc., Chem. Commun.*, (1973) 505–508.

32 V.F. Bystrov and A.U. Stepanyants, *J. Mol. Spectrosc.*, 21 (1966) 241.
33 T.D. Inch, *Annu. Rep. NMR Spectrosc.*, 5A (1972) 316.
34 M. Witanowski, L. Stefaniak, and G.A. Webb, *Annu. Rep. NMR Spectrosc.*, 11B (1981), and references therein.
35 G.A. Olah and T.E. Kiovsky, *J. Am. Chem. Soc.*, 90 (1968) 4666–4672.
36 J. Breg, L.M.J. Kroon-Batenburg, G. Strecker, J. Montreuil, and J.F.G. Vliegenthart, *Eur. J. Biochem.*, 178 (1989) 727–739.
37 P. Dais and A.S. Perlin, *Adv. Carbohydr. Chem. Biochem.*, 45 (1987) 125–168.
38 P. Cagas and C.A. Bush, *Biopolymers*, 30 (1990) 1123–1138.
39 C. Hervé du Penhoat, A. Imberty, N. Roques, V. Michon, J. Mentech, G. Descotes, and S. Perez, *J. Am. Chem. Soc.*, 113 (1991) 3720–3727.
40 A.D. French and J.W. Brady, *ASC Symp. Ser.*, 430 (1990).
41 H. Kovacs, S. Bagley, and J. Kowalewski, *J. Magn. Reson.*, 85 (1989) 530–541.
42 J.P. Carver, *Curr. Opin. Struct. Biol.*, 1 (1991) 716–720.
43 D. Neuhaus and M. Williamson, in *The Nuclear Overhauser Effect in Structural and Conformational Analysis*, VCH Publishers, 1989, p 292.
44 S.N. Ha, A. Giammona, M. Field, and J.W. Brady, *Carbohydr. Res.*, 180 (1988) 207–221.
45 G. Bouchoux, J.P. Flament, and Y. Hoppiliard, *Nouv. J. Chim.*, 7 (1983) 385–390.
46 D. Lamba, D.L. Segre, M. Ragazzi, D.R. Ferro, and T. Toffanin, *Carbohydr. Res.*, 209 (1991) C13–C15.
47 E.T. Olejniczak, R.T. Gampe, Jr., and S.W. Fesik, *J. Magn. Reson.*, 67 (1986) 28–41.